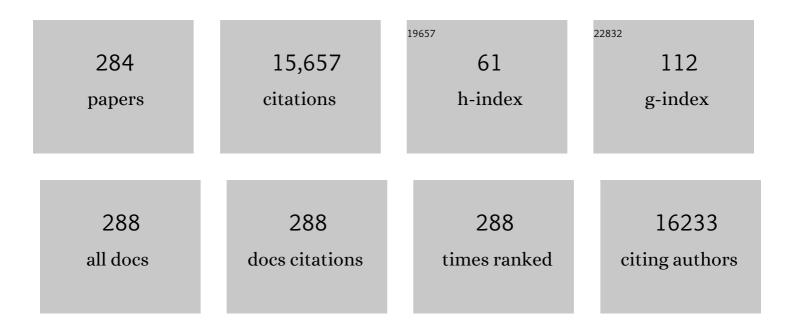
Zou Zhigang

List of Publications by Year in descending order

Source: https://exaly.com/author-pdf/8182890/publications.pdf Version: 2024-02-01



#	Article	IF	CITATIONS
1	An Extrinsic Faradaic Layer on CuSn for High-Performance Electrocatalytic CO ₂ Reduction. CCS Chemistry, 2022, 4, 1610-1618.	7.8	12
2	Photosynthetic microorganisms coupled photodynamic therapy for enhanced antitumor immune effect. Bioactive Materials, 2022, 12, 97-106.	15.6	23
3	Selectively triggering photoelectrons for CO ₂ to CH ₄ reduction over SrTiO ₃ {110} facet with dual-metal sites. Nanotechnology, 2022, 33, 100401.	2.6	4
4	Host/Guest Nanostructured Photoanodes Integrated with Targeted Enhancement Strategies for Photoelectrochemical Water Splitting. Advanced Science, 2022, 9, e2103744.	11.2	31
5	Effects of Co Doping on the Growth and Photocatalytic Properties of ZnO Particles. Molecules, 2022, 27, 833.	3.8	6
6	A high-voltage solar rechargeable device based on a CoPi/BiVO ₄ faradaic junction. Journal of Materials Chemistry A, 2022, 10, 1802-1807.	10.3	6
7	Variable-valence ion and heterointerface accelerated electron transfer kinetics of electrochemical water splitting. Journal of Materials Chemistry A, 2022, 10, 12391-12399.	10.3	21
8	General synthesis of high-entropy alloy and ceramic nanoparticles in nanoseconds. , 2022, 1, 138-146.		91
9	Heat–Electricity Coupling Driven Cascade Oxidation Reaction of Redox Couple and Water. Journal of Physical Chemistry Letters, 2022, 13, 49-57.	4.6	8
10	Effects of transition metal doping on electronic structure of metastable β-Fe ₂ O ₃ photocatalyst for solar-to-hydrogen conversion. Physical Chemistry Chemical Physics, 2022, 24, 6958-6963.	2.8	3
11	FeVO ₄ nanowires for efficient photocatalytic CO ₂ reduction. Catalysis Science and Technology, 2022, 12, 3289-3294.	4.1	12
12	<i>In situ</i> growth of MOF-derived sulfur vacancy-rich CdS nanoparticles on 2D polymers for highly efficient photocatalytic hydrogen generation. Dalton Transactions, 2022, 51, 5841-5858.	3.3	17
13	N-Doped Graphene-Coated Commercial Pt/C Catalysts toward High-Stability and Antipoisoning in Oxygen Reduction Reaction. Journal of Physical Chemistry Letters, 2022, 13, 2019-2026.	4.6	18
14	Bandgap Engineering and Oxygen Vacancies of Ni _{<i>x</i>} V ₂ O _{5+<i>x</i>} (<i>x </i> = 1, 2, 3) for Efficient Visible Lightâ€Đriven CO ₂ to CO with Nearly 100% Selectivity. Solar Rrl, 2022, 6, .	5.8	8
15	Single Pd–S <i>_x</i> Sites <i>In Situ</i> Coordinated on CdS Surface as Efficient Hydrogen Autotransfer Shuttles for Highly Selective Visible-Light-Driven C–N Coupling. ACS Catalysis, 2022, 12, 4481-4490.	11.2	28
16	A Waterâ€Soluble Highly Oxidizing Cobalt Molecular Catalyst Designed for Bioinspired Water Oxidation. Angewandte Chemie - International Edition, 2022, 61, .	13.8	13
17	Symbiotic Algae–Bacteria Dressing for Producing Hydrogen to Accelerate Diabetic Wound Healing. Nano Letters, 2022, 22, 229-237.	9.1	48
18	Boosting O ₂ Reduction and H ₂ O Dehydrogenation Kinetics: Surface <i>N</i> â€Hydroxymethylation of <i>g</i> ₃ N ₄ Photocatalysts for the Efficient Production of H ₂ O ₂ . Advanced Functional Materials, 2022, 32, .	14.9	76

#	Article	IF	CITATIONS
19	Molybdenum Sulfide Quantum Dots Decorated on TiO ₂ for Photocatalytic Hydrogen Evolution. ACS Applied Nano Materials, 2022, 5, 702-709.	5.0	8
20	Boosting photocatalytic CO ₂ reduction <i>via</i> Schottky junction with ZnCr layered double hydroxide nanoflakes aggregated on 2D Ti ₃ C ₂ T _{<i>x</i>} cocatalyst. Nanoscale, 2022, 14, 7538-7546.	5.6	20
21	In-situ synthesis of nickel/palladium bimetal/ZnIn2S4 Schottky heterojunction for efficient photocatalytic hydrogen evolution. Journal of Colloid and Interface Science, 2022, 623, 205-215.	9.4	29
22	Extraterrestrial photosynthesis by Chang'E-5 lunar soil. Joule, 2022, 6, 1008-1014.	24.0	15
23	Deactivation and Stabilization Mechanism of Photothermal CO ₂ Hydrogenation over Black TiO ₂ . ACS Sustainable Chemistry and Engineering, 2022, 10, 6382-6388.	6.7	16
24	Photovoltage memory effect in a portable Faradaic junction solar rechargeable device. Nature Communications, 2022, 13, 2544.	12.8	11
25	High-performance photocatalytic nonoxidative conversion of methane to ethane and hydrogen by heteroatoms-engineered TiO2. Nature Communications, 2022, 13, 2806.	12.8	89
26	Construction of unique heterojunction photoanodes through <i>in situ</i> quasi-epitaxial growth of FeVO ₄ on Fe ₂ O ₃ nanorod arrays for enhanced photoelectrochemical performance. Catalysis Science and Technology, 2022, 12, 4372-4379.	4.1	4
27	Heatâ€Triggered Ferriâ€toâ€Paramagnetic Transition Accelerates Redox Coupleâ€Mediated Electrocatalytic Water Oxidation. Advanced Functional Materials, 2022, 32, .	14.9	8
28	Homogeneous solution assembled Turing structures with near zero strain semi-coherence interface. Nature Communications, 2022, 13, .	12.8	13
29	An energy level alignment strategy to boost the open-circuit voltage via a Mg:TiO2 compact layer in the planar heterojunction CsPbBr3 solar cells. Applied Physics Letters, 2022, 120, .	3.3	5
30	Centimeter-scale perovskite SrTaO2N single crystals with enhanced photoelectrochemical performance. Science Bulletin, 2022, 67, 1458-1466.	9.0	6
31	Exploring N-Containing Compound Catalyst for H2S Selective Oxidation: Case Study of TaON and Ta3N5. Catalysis Letters, 2021, 151, 1728-1737.	2.6	2
32	A Capacitorâ€ŧype Faradaic Junction for Direct Solar Energy Conversion and Storage. Angewandte Chemie - International Edition, 2021, 60, 1390-1395.	13.8	19
33	A Capacitorâ€ŧype Faradaic Junction for Direct Solar Energy Conversion and Storage. Angewandte Chemie, 2021, 133, 1410-1415.	2.0	1
34	Beyond C ₃ N ₄ π-conjugated metal-free polymeric semiconductors for photocatalytic chemical transformations. Chemical Society Reviews, 2021, 50, 2147-2172.	38.1	118
35	Stateâ€ofâ€ŧheâ€Art Progress in Diverse Black Phosphorusâ€Based Structures: Basic Properties, Synthesis, Stability, Photo―and Electrocatalysisâ€Driven Energy Conversion. Advanced Functional Materials, 2021, 31, 2005197.	14.9	40
36	Ultrathin Z-scheme 2D/2D N-doped HTiNbO5 nanosheets/g-C3N4 porous composites for efficient photocatalytic degradation and H2 generation under visible light. Journal of Colloid and Interface Science, 2021, 583, 58-70.	9.4	59

#	Article	IF	CITATIONS
37	Shedding light on <scp>CO₂</scp> : Catalytic synthesis of solar methanol. EcoMat, 2021, 3, e12078.	11.9	13
38	Bimetallic oxyhydroxide <i>in situ</i> derived from an Fe ₂ Co-MOF for efficient electrocatalytic oxygen evolution. Journal of Materials Chemistry A, 2021, 9, 13271-13278.	10.3	27
39	Simple fabrication of Z-scheme MgIn ₂ S ₄ /Bi ₂ WO ₆ hierarchical heterostructures for enhancing photocatalytic reduction of Cr(<scp>vi</scp>). Catalysis Science and Technology, 2021, 11, 6271-6280.	4.1	15
40	Ultrafast Fenton-like reaction route to FeOOH/NiFe-LDH heterojunction electrode for efficient oxygen evolution reaction. Journal of Materials Chemistry A, 2021, 9, 21785-21791.	10.3	55
41	Electrocatalytic fixation of N ₂ into NO ₃ ^{â^'} : electron transfer between oxygen vacancies and loaded Au in Nb ₂ O _{5â^'<i>x</i>} nanobelts to promote ambient nitrogen oxidation. Journal of Materials Chemistry A, 2021, 9, 17442-17450.	10.3	33
42	Do Cu Substrates Participate in Bi Electrocatalytic CO ₂ Reduction?. ChemNanoMat, 2021, 7, 128-133.	2.8	6
43	Understanding the enhanced catalytic activity of high entropy alloys: from theory to experiment. Journal of Materials Chemistry A, 2021, 9, 19410-19438.	10.3	43
44	α-Fe ₂ O ₃ /Ag/CdS ternary heterojunction photoanode for efficient solar water oxidation. Catalysis Science and Technology, 2021, 11, 5859-5867.	4.1	7
45	A strategy of asymmetric local structure based on mesoporous MoO ₂ toward efficient electrocatalysis. Chemical Communications, 2021, 57, 7834-7837.	4.1	3
46	Visible-light-responsive Z-scheme system for photocatalytic lignocellulose-to-H ₂ conversion. Chemical Communications, 2021, 57, 9898-9901.	4.1	12
47	Layered BiOCl/H ⁺ TiNbO ₅ ^{â^'} heterojunctions for boosting visible-light-driven photocatalytic RhB degradation. Sustainable Energy and Fuels, 2021, 5, 4680-4689.	4.9	14
48	Photocatalytic and Thermocatalytic Conversion of Methane. Solar Rrl, 2021, 5, 2000596.	5.8	16
49	Photocatalytic Hydrogen Production by Stable CsPbBr ₃ @PANI Nanoparticles in Aqueous Solution. ChemCatChem, 2021, 13, 1711-1716.	3.7	15
50	Ureaâ€Assisted Synthesis and Tailoring Cobalt Cores for Synergetic Promotion of Hydrogen Evolution Reaction in Acid and Alkaline Media. Advanced Energy and Sustainability Research, 2021, 2, 2000091.	5.8	5
51	Promotion effect of metal phosphides towards electrocatalytic and photocatalytic water splitting. EcoMat, 2021, 3, e12097.	11.9	46
52	Material Design and Surface/Interface Engineering of Photoelectrodes for Solar Water Splitting. Solar Rrl, 2021, 5, 2100100.	5.8	33
53	Elegant Construction of ZnIn ₂ S ₄ /BiVO ₄ Hierarchical Heterostructures as Direct Z-Scheme Photocatalysts for Efficient CO ₂ Photoreduction. ACS Applied Materials & Interfaces, 2021, 13, 15092-15100.	8.0	115
54	3D Hydrangeaâ€like InVO ₄ /Ti ₃ C ₂ T _x Hierarchical Heterosystem Collaborating with 2D/2D Interface Interaction for Enhanced Photocatalytic CO ₂ Reduction. ChemNanoMat, 2021, 7, 815-823.	2.8	14

#	Article	IF	CITATIONS
55	Direct Observation of Heterogeneous Surface Reactivity and Reconstruction on Terminations of Grain Boundaries of Platinum. , 2021, 3, 622-629.		14
56	An ultraviolet-ozone post-treatment to remove the inherent impurities in all-ambient solution-processed CsPbBr3 perovskite films. Applied Physics Letters, 2021, 118, 221604.	3.3	5
57	Suppressing the Defects in CsPbl2Br Perovskite Photovoltaic Films via a Homogeneous Cap-Mediated Annealing Strategy. Energy & Fuels, 2021, 35, 11488-11495.	5.1	4
58	Extraterrestrial artificial photosynthetic materials for <i>in-situ</i> resource utilization. National Science Review, 2021, 8, nwab104.	9.5	17
59	Robust Molecular Dipoleâ€Enabled Defect Passivation and Control of Energyâ€Level Alignment for Highâ€Efficiency Perovskite Solar Cells. Angewandte Chemie - International Edition, 2021, 60, 17664-17670.	13.8	69
60	Direct Electrochemical Protonation of Metal Oxide Particles. Journal of the American Chemical Society, 2021, 143, 9236-9243.	13.7	25
61	Solarâ€Driven Lignocelluloseâ€ŧoâ€H ₂ Conversion in Water using 2Dâ€2D MoS ₂ /TiO ₂ Photocatalysts. ChemSusChem, 2021, 14, 2860-2865.	6.8	27
62	Advancing solar energy conversion materials: fuel the future. National Science Review, 2021, 8, nwab128.	9.5	2
63	Vacancy-defect modulated pathway of photoreduction of CO2 on single atomically thin AgInP2S6 sheets into olefiant gas. Nature Communications, 2021, 12, 4747.	12.8	128
64	Hollow InVO ₄ Nanocuboid Assemblies toward Promoting Photocatalytic N ₂ Conversion Performance. Advanced Materials, 2021, 33, e2006780.	21.0	38
65	2D Highâ€Entropy Hydrotalcites. Small, 2021, 17, e2103412.	10.0	27
66	Vertical Graphene Arrays as Electrodes for Ultraâ€High Energy Density AC Lineâ€Filtering Capacitors. Angewandte Chemie, 2021, 133, 24710-24714.	2.0	7
67	<i>In situ</i> construction of a 2D/2D heterostructured Znln ₂ S ₄ /Bi ₂ MoO ₆ <i>Z</i> boosting the photoreduction activity of Cr(<scp>vi</scp>). Catalysis Science and Technology, 2021, 11, 3885-3893.	4.1	30
68	Lanthanum bismuth oxide photocatalysts for CO ₂ reduction to CO with high selectivity. Sustainable Energy and Fuels, 2021, 5, 2688-2694.	4.9	6
69	Carrier Mobility Enhancement in (121)-Oriented CsPbBr ₃ Perovskite Films Induced by the Microstructure Tailoring of PbBr ₂ Precursor Films. ACS Applied Electronic Materials, 2021, 3, 373-384.	4.3	30
70	Constructing spin pathways in LaCoO3 by Mn substitution to promote oxygen evolution reaction. Applied Physics Letters, 2021, 119, .	3.3	12
71	Thermally Stable Allâ€Perovskite Tandem Solar Cells Fully Using Metal Oxide Charge Transport Layers and Tunnel Junction. Solar Rrl, 2021, 5, 2100814.	5.8	24
72	Direct Z-scheme hierarchical heterostructures of oxygen-doped g-C ₃ N ₄ /In ₂ S ₃ with efficient photocatalytic Cr(<scp>vi</scp>) reduction activity. Catalysis Science and Technology, 2021, 11, 7963-7972.	4.1	13

#	Article	IF	CITATIONS
73	Faradaic junction and isoenergetic charge transfer mechanism on semiconductor/semiconductor interfaces. Nature Communications, 2021, 12, 6363.	12.8	14
74	In Situ Determination of Polaron-Mediated Ultrafast Electron Trapping in Rutile TiO ₂ Nanorod Photoanodes. Journal of Physical Chemistry Letters, 2021, 12, 10815-10822.	4.6	14
75	Bismuth Vacancy-Induced Efficient CO ₂ Photoreduction in BiOCl Directly from Natural Air: A Progressive Step toward Photosynthesis in Nature. Nano Letters, 2021, 21, 10260-10266.	9.1	74
76	Spin unlocking oxygen evolution reaction on antiperovskite nitrides. Journal of Materials Chemistry A, 2021, 9, 25435-25444.	10.3	19
77	Unconventional Route to Oxygenâ€Vacancyâ€Enabled Highly Efficient Electron Extraction and Transport in Perovskite Solar Cells. Angewandte Chemie - International Edition, 2020, 59, 1611-1618.	13.8	104
78	Unconventional Route to Oxygenâ€Vacancyâ€Enabled Highly Efficient Electron Extraction and Transport in Perovskite Solar Cells. Angewandte Chemie, 2020, 132, 1628-1635.	2.0	34
79	Inhibiting Hydrogen Evolution using a Chloride Adlayer for Efficient Electrochemical CO ₂ Reduction on Zn Electrodes. ACS Applied Materials & Interfaces, 2020, 12, 4565-4571.	8.0	49
80	Silicon Photoanode Modified with Workâ€functionâ€tuned Ni@Fe _{<i>y</i>} Ni _{1â^'<i>y</i>} (OH) ₂ Coreâ€5hell Particles for Water Oxidation. ChemSusChem, 2020, 13, 6037-6044.	6.8	11
81	ALD-grown oxide protective layers on Ta3N5–Cu2O n–p nanoarray heterojunction for improved photoelectrochemical water splitting. Applied Physics Letters, 2020, 117, 163902.	3.3	13
82	Curing the fundamental issue of impurity phases in two-step solution-processed CsPbBr3 perovskite films. Science Bulletin, 2020, 65, 726-737.	9.0	34
83	Modulation of Disordered Coordination Degree Based on Surface Defective Metal–Organic Framework Derivatives toward Boosting Oxygen Evolution Electrocatalysis. Small, 2020, 16, e2003630.	10.0	44
84	Passivation Strategy of Reducing Both Electron and Hole Trap States for Achieving High-Efficiency PbS Quantum-Dot Solar Cells with Power Conversion Efficiency over 12%. ACS Energy Letters, 2020, 5, 3224-3236.	17.4	49
85	In Situ-Grown Island-Shaped Hollow Graphene on TaON with Spatially Separated Active Sites Achieving Enhanced Visible-Light CO ₂ Reduction. ACS Catalysis, 2020, 10, 15083-15091.	11.2	51
86	Artificial Trees for Artificial Photosynthesis: Construction of Dendrite-Structured α-Fe ₂ O ₃ /g-C ₃ N ₄ Z-Scheme System for Efficient CO ₂ Reduction into Solar Fuels. ACS Applied Energy Materials, 2020, 3, 6561-6572.	5.1	67
87	Anchoring of black phosphorus quantum dots onto WO ₃ nanowires to boost photocatalytic CO ₂ conversion into solar fuels. Chemical Communications, 2020, 56, 7777-7780.	4.1	57
88	Mildly regulated intrinsic faradaic layer at the oxide/water interface for improved photoelectrochemical performance. Chemical Science, 2020, 11, 6297-6304.	7.4	15
89	Reversible Charge Transfer and Adjustable Potential Window in Semiconductor/Faradaic Layer/Liquid Junctions. IScience, 2020, 23, 100949.	4.1	17
90	CoS ₂ @N-doped carbon core–shell nanorod array grown on Ni foam for enhanced electrocatalytic water oxidation. Journal of Materials Chemistry A, 2020, 8, 6795-6803.	10.3	75

#	Article	IF	CITATIONS
91	Constructing N-Doped KNb3O8/g-C3N4 Composite for Efficient Photocatalytic H2 Generation and Degradation under Visible Light Irradiation. Catalysis Letters, 2020, 150, 2798-2806.	2.6	5
92	Few-Layer Black Phosphorus Nanosheets: A Metal-Free Cocatalyst for Photocatalytic Nitrogen Fixation. ACS Applied Materials & Interfaces, 2020, 12, 17343-17352.	8.0	74
93	Super stable CsPbBr3@SiO2 tumor imaging reagent by stress-response encapsulation. Nano Research, 2020, 13, 795-801.	10.4	55
94	Paving the road toward the use of Î ² -Fe2O3 in solar water splitting: Raman identification, phase transformation and strategies for phase stabilization. National Science Review, 2020, 7, 1059-1067.	9.5	38
95	Polyimide-based photocatalysts: rational design for energy and environmental applications. Journal of Materials Chemistry A, 2020, 8, 14441-14462.	10.3	38
96	Frontispiz: Unconventional Route to Oxygenâ€Vacancyâ€Enabled Highly Efficient Electron Extraction and Transport in Perovskite Solar Cells. Angewandte Chemie, 2020, 132, .	2.0	0
97	Suppression of Point Defects for Band Edge Engineering in a Semiconducting Photocatalyst. Journal of Physical Chemistry Letters, 2020, 11, 1708-1713.	4.6	11
98	Room Temperature Surface Modification of Ultrathin FeOOH Cocatalysts on Fe ₂ O ₃ Photoanodes for High Photoelectrochemical Water Splitting. Journal of Nanomaterials, 2020, 2020, 1-7.	2.7	13
99	Frontispiece: Unconventional Route to Oxygenâ€Vacancyâ€Enabled Highly Efficient Electron Extraction and Transport in Perovskite Solar Cells. Angewandte Chemie - International Edition, 2020, 59, .	13.8	1
100	2D Titanium/Niobium Metal Oxideâ€Based Materials for Photocatalytic Application. Solar Rrl, 2020, 4, 2000070.	5.8	34
101	Simultaneous Optimization of Phase and Morphology of CsPbBr 3 Films via Controllable Ostwald Ripening by Ethylene Glycol Monomethylether/Isopropanol Biâ€Solvent Engineering. Advanced Engineering Materials, 2020, 22, 2000162.	3.5	19
102	Facile grafting strategy synthesis of single-atom electrocatalyst with enhanced ORR performance. Nano Research, 2020, 13, 1519-1526.	10.4	60
103	Polaron States as a Massive Electron-Transfer Pathway at Heterojunction Interface. Journal of Physical Chemistry Letters, 2020, 11, 9184-9194.	4.6	14
104	<i>In situ</i> preparation of Bi ₂ S ₃ nanoribbon-anchored BiVO ₄ nanoscroll heterostructures for the catalysis of Cr(<scp>vi</scp>) photoreduction. Catalysis Science and Technology, 2020, 10, 3843-3847.	4.1	14
105	Lowâ€Workâ€Function Silver Activating Nâ€doped Graphene as Efficient Oxygen Reduction Catalysts in Acidic Medium. ChemCatChem, 2019, 11, 1033-1038.	3.7	9
106	<i>In situ</i> formed oxy/hydroxide antennas accelerating the water dissociation kinetics on a Co@N-doped carbon core–shell assembly for hydrogen production in alkaline solution. Dalton Transactions, 2019, 48, 11927-11933.	3.3	6
107	Incorporating <i>p</i> â€Phenylene as an Electronâ€Donating Group into Graphitic Carbon Nitride for Efficient Charge Separation. ChemSusChem, 2019, 12, 4285-4292.	6.8	22
108	Elegant Molecular Iodine/Antisolvent Solution Engineering To Tune the Fermi Level of Perovskite CH ₃ NH ₃ PbI ₃ . ACS Applied Energy Materials, 2019, 2, 5753-5758.	5.1	7

#	Article	IF	CITATIONS
109	Co–P Bonds as Atomic-Level Charge Transfer Channel To Boost Photocatalytic H ₂ Production of Co ₂ P/Black Phosphorus Nanosheets Photocatalyst. ACS Catalysis, 2019, 9, 7801-7807.	11.2	124
110	Ta ₃ N ₅ nanorods encapsulated into 3D hydrangea-like MoS ₂ for enhanced photocatalytic hydrogen evolution under visible light irradiation. Dalton Transactions, 2019, 48, 13176-13183.	3.3	27
111	Effect of Bulk Hydrogen on the Photocatalytic Activity of Semiconducting Ta ₃ N ₅ : A Hybrid-DFT Viewpoint. Journal of Physical Chemistry C, 2019, 123, 28763-28768.	3.1	7
112	Schottky junction effect enhanced plasmonic photocatalysis by TaON@Ni NP heterostructures. Chemical Communications, 2019, 55, 11754-11757.	4.1	52
113	Near 100% selectivity for visible-light-driven CO2 reduction to CH4 on a dual-metal site photocatalyst. Science China Chemistry, 2019, 62, 1553-1554.	8.2	5
114	Hollow BiVO4/Bi2S3 cruciate heterostructures with enhanced visible-light photoactivity. Catalysis Science and Technology, 2019, 9, 182-187.	4.1	13
115	Lewis acid activated CO ₂ reduction over a Ni modified Ni–Ge hydroxide driven by visible-infrared light. Dalton Transactions, 2019, 48, 1672-1679.	3.3	12
116	Defect Engineering in Semiconductors: Manipulating Nonstoichiometric Defects and Understanding Their Impact in Oxynitrides for Solar Energy Conversion. Advanced Functional Materials, 2019, 29, 1808389.	14.9	56
117	Boosting the hydrogen evolution performance of a ternary Mo _x Co _{1â^'x} P nanowire array by tuning the Mo/Co ratio. Journal of Materials Chemistry A, 2019, 7, 14842-14848.	10.3	36
118	Three-Dimensional Functionalized Carbon Nanotubes/Graphitic Carbon Nitride Hybrid Composite as the Sulfur Host for High-Performance Lithium–Sulfur Batteries. Journal of Physical Chemistry C, 2019, 123, 15924-15934.	3.1	18
119	Design Principles for Construction of Charge Transport Channels in Particle-Assembled Water-Splitting Photoelectrodes. ACS Sustainable Chemistry and Engineering, 2019, 7, 10509-10515.	6.7	13
120	An Integrated Single-Electrode Method Reveals the Template Roles of Atomic Steps: Disturb Interfacial Water Networks and Thus Affect the Reactivity of Electrocatalysts. Journal of the American Chemical Society, 2019, 141, 8516-8526.	13.7	20
121	Porphyrin ontaining Polyimide with Enhanced Light Absorption and Photocatalysis Activity. Chemistry - an Asian Journal, 2019, 14, 2138-2148.	3.3	23
122	Highly selective electrochemical CO ₂ reduction to CO using a redox-active couple on low-crystallinity mesoporous ZnGa ₂ O ₄ catalyst. Journal of Materials Chemistry A, 2019, 7, 9316-9323.	10.3	30
123	Interfacial Effects on the Band Edges of Ta3N5 Photoanodes in an Aqueous Environment: A Theoretical View. IScience, 2019, 13, 432-439.	4.1	10
124	Convincing Synthesis of Atomically Thin, Single-Crystalline InVO ₄ Sheets toward Promoting Highly Selective and Efficient Solar Conversion of CO ₂ into CO. Journal of the American Chemical Society, 2019, 141, 4209-4213.	13.7	199
125	Ultrathin nanosheet-anchored hexahedral prismatic Bi ₂ MoO ₆ arrays: one-step constructed and crystal facet-based homojunctions boosting photocatalytic CO ₂ reduction and N ₂ fixation. Catalysis Science and Technology, 2019, 9, 7045-7050.	4.1	11
126	Silicon photoanodes partially covered by Ni@Fe core-shell particles with <i>in situ</i> formed gradient-enhanced junction electric field for photoelectrochemical water oxidation. Applied Physics Letters, 2019, 115, .	3.3	4

#	Article	IF	CITATIONS
127	Core-Shell Heterostructured and Visible-Light-Driven Titanoniobate/TiO2 Composite for Boosting Photodegradation Performance. Nanomaterials, 2019, 9, 1503.	4.1	6
128	Heterogeneous degradation of organic contaminants in the photo-Fenton reaction employing pure cubic β-Fe2O3. Applied Catalysis B: Environmental, 2019, 245, 410-419.	20.2	107
129	Carbon Nanotube@RuO ₂ as a High Performance Catalyst for Li–CO ₂ Batteries. ACS Applied Materials & Interfaces, 2019, 11, 5146-5151.	8.0	70
130	Reactive Inorganic Vapor Deposition of Perovskite Oxynitride Films for Solar Energy Conversion. Research, 2019, 2019, 9282674.	5.7	17
131	Oriented attachment growth of hundred-nanometer-size LaTaON ₂ single crystals in molten salts for enhanced photoelectrochemical water splitting. Journal of Materials Chemistry A, 2018, 6, 7706-7713.	10.3	26
132	Tuning spontaneous polarization to alter water oxidation/reduction activities of LiNbO3. Applied Physics Letters, 2018, 112, .	3.3	11
133	Solvothermal synthesis of porous conjugated polymer with high surface area for efficient adsorption of organic and biomolecules. Journal of Porous Materials, 2018, 25, 1659-1668.	2.6	5
134	Flux synthesis of regular Bi ₄ TaO ₈ Cl square nanoplates exhibiting dominant exposure surfaces of {001} crystal facets for photocatalytic reduction of CO ₂ to methane. Nanoscale, 2018, 10, 1905-1911.	5.6	41
135	Polymerizable ionic liquid as a precursor for N, P co-doped carbon toward the oxygen reduction reaction. Catalysis Science and Technology, 2018, 8, 1142-1150.	4.1	44
136	Rational design of electrocatalysts for simultaneously promoting bulk charge separation and surface charge transfer in solar water splitting photoelectrodes. Journal of Materials Chemistry A, 2018, 6, 2568-2576.	10.3	56
137	Controllable Conformation Transfer of Conjugated Polymer toward High Photoelectrical Performance: The Role of Solvent in Induced-Crystallization Route. Journal of Physical Chemistry C, 2018, 122, 1037-1043.	3.1	10
138	Unlocking the potential of graphene for water oxidation using an orbital hybridization strategy. Energy and Environmental Science, 2018, 11, 407-416.	30.8	52
139	Promoted photoelectrochemical activity of BiVO4 coupled with LaFeO3 and LaCoO3. Research on Chemical Intermediates, 2018, 44, 1013-1024.	2.7	10
140	Interface Manipulation to Improve Plasmonâ€Coupled Photoelectrochemical Water Splitting on αâ€Fe ₂ O ₃ Photoanodes. ChemSusChem, 2018, 11, 237-244.	6.8	38
141	Polyhedral 30â€Faceted BiVO ₄ Microcrystals Predominantly Enclosed by Highâ€Index Planes Promoting Photocatalytic Waterâ€Splitting Activity. Advanced Materials, 2018, 30, 1703119.	21.0	155
142	Oxygen-Vacancy-Activated CO ₂ Splitting over Amorphous Oxide Semiconductor Photocatalyst. ACS Catalysis, 2018, 8, 516-525.	11.2	126
143	Tandem photoelectrochemical cells for solar water splitting. Advances in Physics: X, 2018, 3, 1487267.	4.1	25
144	Two-Step Synthesis of Laminar Vanadate via a Facile Hydrothermal Route and Enhancing the Photocatalytic Reduction of CO ₂ into Solar Fuel through Tuning of the Oxygen Vacancies by in Situ Vacuum Illumination Treatment. ACS Applied Energy Materials, 2018, 1, 6857-6864.	5.1	9

#	Article	IF	CITATIONS
145	Direct storage of holes in ultrathin Ni(OH) ₂ on Fe ₂ O ₃ photoelectrodes for integrated solar charging battery-type supercapacitors. Journal of Materials Chemistry A, 2018, 6, 21360-21367.	10.3	44
146	Facet-Dependent Enhancement in the Activity of Bismuth Vanadate Microcrystals for the Photocatalytic Conversion of Methane to Methanol. ACS Applied Nano Materials, 2018, 1, 6683-6691.	5.0	79
147	Room-Temperature Preparation of Cobalt-Based Electrocatalysts through Simple Solution Treatment for Selectively High-Efficiency Hydrogen Evolution Reaction in Alkaline or Acidic Medium. Journal of Nanomaterials, 2018, 2018, 1-9.	2.7	2
148	Frustrated Lewis Pairs Accelerating CO ₂ Reduction on Oxyhydroxide Photocatalysts with Surface Lattice Hydroxyls as a Solidâ€6tate Proton Donor. Advanced Functional Materials, 2018, 28, 1804191.	14.9	102
149	Improved water-splitting performances of CuW1â^'xMoxO4 photoanodes synthesized by spray pyrolysis. Science China Materials, 2018, 61, 1297-1304.	6.3	22
150	Surface chemistry imposes selective reduction of CO ₂ to CO over Ta ₃ N ₅ /LaTiO ₂ N photocatalyst. Journal of Materials Chemistry A, 2018, 6, 14838-14846.	10.3	34
151	Oriented Growth of Sc-Doped Ta ₃ N ₅ Nanorod Photoanode Achieving Low-Onset-Potential for Photoelectrochemical Water Oxidation. ACS Applied Energy Materials, 2018, 1, 4150-4157.	5.1	46
152	Lead Selenide Colloidal Quantum Dot Solar Cells Achieving High Open-Circuit Voltage with One-Step Deposition Strategy. Journal of Physical Chemistry Letters, 2018, 9, 3598-3603.	4.6	38
153	A Facetâ€Dependent Schottkyâ€Junction Electron Shuttle in a BiVO ₄ {010}–Au–Cu ₂ O Zâ€Scheme Photocatalyst for Efficient Charge Separation. Advanced Functional Materials, 2018, 28, 1801214.	14.9	193
154	In-Situ Formed Hydroxide Accelerating Water Dissociation Kinetics on Co ₃ N for Hydrogen Production in Alkaline Solution. ACS Applied Materials & Interfaces, 2018, 10, 22102-22109.	8.0	54
155	Coprecipitation-Gel Synthesis and Degradation Mechanism of Octahedral Li _{1.2} Mn _{0.54} Ni _{0.13} Co _{0.13} O ₂ as High-Performance Cathode Materials for Lithium-Ion Batteries. ACS Applied Materials & amp; Interfaces, 2018, 10, 23018-23028.	8.0	15
156	Confinement effect of monolayer MoS ₂ quantum dots on conjugated polyimide and promotion of solar-driven photocatalytic hydrogen generation. Dalton Transactions, 2017, 46, 3877-3886.	3.3	72
157	Effects of Mg–Zr codoping on the photoelectrochemical properties of a Ta ₃ N ₅ semiconductor: a theoretical insight. Journal of Materials Chemistry A, 2017, 5, 6966-6973.	10.3	19
158	Series of ZnSn(OH) ₆ Polyhedra: Enhanced CO ₂ Dissociation Activation and Crystal Facet-Based Homojunction Boosting Solar Fuel Synthesis. Inorganic Chemistry, 2017, 56, 5704-5709.	4.0	27
159	A novel wide-spectrum response hexagonal YFeO ₃ photoanode for solar water splitting. RSC Advances, 2017, 7, 18418-18420.	3.6	18
160	Cathodic shift of a photo-potential on a Ta ₃ N ₅ photoanode by post-heating a TiO ₂ passivation layer. RSC Advances, 2017, 7, 30650-30656.	3.6	8
161	Silicon Photoanodes Partially Covered by Ni@Ni(OH) ₂ Core–Shell Particles for Photoelectrochemical Water Oxidation. ChemSusChem, 2017, 10, 2897-2903.	6.8	58
162	Temperature-controlled evolution of microstructures that promote charge separation in a TaON photoanode for enhanced solar energy conversion. Journal of Materials Chemistry A, 2017, 5, 12848-12855.	10.3	24

#	Article	IF	CITATIONS
163	A facile spray pyrolysis method to prepare Ti-doped ZnFe ₂ O ₄ for boosting photoelectrochemical water splitting. Journal of Materials Chemistry A, 2017, 5, 7571-7577.	10.3	113
164	Tuning the ion permeability of an Al ₂ O ₃ coating layer on Fe ₂ O ₃ photoanodes for improved photoelectrochemical water oxidation. Journal of Materials Chemistry A, 2017, 5, 8402-8407.	10.3	54
165	Pt nanocrystals electrodeposited on reduced graphene oxide/carbon fiber paper with efficient electrocatalytic properties. Progress in Natural Science: Materials International, 2017, 27, 452-459.	4.4	6
166	Two-dimensional nanomaterials for photocatalytic CO ₂ reduction to solar fuels. Sustainable Energy and Fuels, 2017, 1, 1875-1898.	4.9	156
167	Bi ₂ MoO ₆ Nanostrip Networks for Enhanced Visibleâ€Light Photocatalytic Reduction of CO ₂ to CH ₄ . ChemPhysChem, 2017, 18, 3240-3244.	2.1	38
168	Mg-doped Ta ₃ N ₅ nanorods coated with a conformal CoOOH layer for water oxidation: bulk and surface dual modification of photoanodes. Journal of Materials Chemistry A, 2017, 5, 20439-20447.	10.3	49
169	Back Electron Transfer at TiO ₂ Nanotube Photoanodes in the Presence of a H ₂ O ₂ Hole Scavenger. ACS Applied Materials & Interfaces, 2017, 9, 33887-33895.	8.0	31
170	Threeâ€Dimensional Hierarchical Architectures Derived from Surfaceâ€Mounted Metal–Organic Framework Membranes for Enhanced Electrocatalysis. Angewandte Chemie - International Edition, 2017, 56, 13781-13785.	13.8	193
171	La ₂ O ₃ â€Modified LaTiO ₂ N Photocatalyst with Spatially Separated Active Sites Achieving Enhanced CO ₂ Reduction. Advanced Functional Materials, 2017, 27, 1702447.	14.9	87
172	Interfaceâ€Engineered Ni(OH) ₂ /βâ€like FeOOH Electrocatalysts for Highly Efficient and Stable Oxygen Evolution Reaction. Chemistry - an Asian Journal, 2017, 12, 2720-2726.	3.3	43
173	An easily modified method using FeCl3 to synthesize nanoporous gold with a high surface area. RSC Advances, 2017, 7, 18327-18332.	3.6	5
174	Investigating the Role of Tunable Nitrogen Vacancies in Graphitic Carbon Nitride Nanosheets for Efficient Visible-Light-Driven H ₂ Evolution and CO ₂ Reduction. ACS Sustainable Chemistry and Engineering, 2017, 5, 7260-7268.	6.7	322
175	Threeâ€Dimensional Hierarchical Architectures Derived from Surfaceâ€Mounted Metal–Organic Framework Membranes for Enhanced Electrocatalysis. Angewandte Chemie, 2017, 129, 13969-13973.	2.0	42
176	Hydrogen Evolution Reaction of Î ³ -Mo0.5W0.5 C Achieved by High Pressure High Temperature Synthesis. Catalysts, 2016, 6, 208.	3.5	3
177	Enhanced InGaN/GaN photoelectrodes for visibleâ€lightâ€driven hydrogen generation by surface roughening. Physica Status Solidi (A) Applications and Materials Science, 2016, 213, 2704-2708.	1.8	1
178	Fabrication of Oxygenâ€Doped Doubleâ€Shelled GaN Hollow Spheres toward Efficient Photoreduction of CO ₂ . Particle and Particle Systems Characterization, 2016, 33, 583-588.	2.3	13
179	Nonequilibrium Ti ⁴⁺ Doping Significantly Enhances the Performance of Fe ₂ O ₃ Photoanodes by Quenching. ChemNanoMat, 2016, 2, 652-655.	2.8	11
180	A perspective on perovskite oxide semiconductor catalysts for gas phase photoreduction of carbon dioxide. MRS Communications, 2016, 6, 216-225.	1.8	18

#	Article	IF	CITATIONS
181	Coarsening of one-step deposited organolead triiodide perovskite films via Ostwald ripening for high efficiency planar-heterojunction solar cells. Dalton Transactions, 2016, 45, 7856-7865.	3.3	53
182	Ultralong metahewettite CaV 6 O 16 ·3H 2 O nanoribbons as novel host materials for lithium storage: Towards high-rate and excellent long-term cyclability. Nano Energy, 2016, 22, 38-47.	16.0	38
183	Photocatalytic reduction of CO ₂ over Ag/TiO ₂ nanocomposites prepared with a simple and rapid silver mirror method. Nanoscale, 2016, 8, 11870-11874.	5.6	139
184	Enhanced Waterâ€Splitting Performance of Perovskite SrTaO ₂ N Photoanode Film through Ameliorating Interparticle Charge Transport. Advanced Functional Materials, 2016, 26, 7156-7163.	14.9	86
185	Solid Solution Photocatalyst with Spontaneous Polarization Exhibiting Low Recombination Toward Efficient CO ₂ Photoreduction. ChemSusChem, 2016, 9, 2064-2068.	6.8	17
186	Construction and Nanoscale Detection of Interfacial Charge Transfer of Elegant Z-Scheme WO ₃ /Au/In ₂ S ₃ Nanowire Arrays. Nano Letters, 2016, 16, 5547-5552.	9.1	217
187	Highly Flexible Self-Powered Organolead Trihalide Perovskite Photodetectors with Gold Nanowire Networks as Transparent Electrodes. ACS Applied Materials & Interfaces, 2016, 8, 23868-23875.	8.0	95
188	Anatase Mg0.05Ta0.95O1.15N0.85: a novel photocatalyst for solar hydrogen production. RSC Advances, 2016, 6, 86240-86244.	3.6	5
189	Microstructure modulation of the CH3NH3PbI3 layer in perovskite solar cells by 2-propanol pre-wetting and annealing in a spray-assisted solution process. Journal of Materials Chemistry A, 2016, 4, 11372-11380.	10.3	17
190	Effect of nitrogen-doped PtRu/graphene catalyst on its activity and durability for methanol oxidation. Journal of Applied Electrochemistry, 2016, 46, 895-900.	2.9	16
191	Photoelectrochemical cell for unassisted overall solar water splitting using a BiVO ₄ photoanode and Si nanoarray photocathode. RSC Advances, 2016, 6, 9905-9910.	3.6	64
192	One-step growth of 3D CoNi ₂ S ₄ nanorods and cross-linked NiCo ₂ S ₄ nanosheet arrays on carbon paper as anodes for high-performance lithium ion batteries. Chemical Communications, 2016, 52, 5258-5261.	4.1	49
193	Laser-assisted crystallization of CH ₃ NH ₃ PbI ₃ films for efficient perovskite solar cells with a high open-circuit voltage. Chemical Communications, 2016, 52, 5394-5397.	4.1	49
194	Aging Precursor Solution in High Humidity Remarkably Promoted Grain Growth in Cu ₂ ZnSnS ₄ Films. ACS Applied Materials & Interfaces, 2016, 8, 5432-5438.	8.0	34
195	Theoretical study on the surface stabilities, electronic structures and water adsorption behavior of the Ta ₃ N ₅ (110) surface. Physical Chemistry Chemical Physics, 2016, 18, 7938-7945.	2.8	8
196	In situ direct growth of single crystalline metal (Co, Ni) selenium nanosheets on metal fibers as counter electrodes toward low-cost, high-performance fiber-shaped dye-sensitized solar cells. Nanoscale, 2016, 8, 2304-2308.	5.6	28
197	Significant improvements in InGaN/GaN nano-photoelectrodes for hydrogen generation by structure and polarization optimization. Scientific Reports, 2016, 6, 20218.	3.3	27
198	Construction and Nanoscale Detection of Interfacial Charge Transfer of Elegant Z-Scheme WO/Au/InS Nanowire Arrays. Nano Letters, 2016, , .	9.1	0

#	Article	IF	CITATIONS
199	Enhancement of Photoelectrochemical Performance in Water Oxidation over Bismuth Vanadate Photoanodes by Incorporation with Reduced Graphene Oxide. ChemCatChem, 2015, 7, 2979-2985.	3.7	11
200	Selective etching of metastable phase induced an efficient Culn _{0.7} Ga _{0.3} S ₂ nano-photocathode for solar water splitting. Journal of Materials Chemistry A, 2015, 3, 7840-7848.	10.3	33
201	Stateâ€ofâ€ŧheâ€Art Progress in Diverse Heterostructured Photocatalysts toward Promoting Photocatalytic Performance. Advanced Functional Materials, 2015, 25, 998-1013.	14.9	706
202	Construction of Visible-Light-Responsive SrTiO3 with Enhanced CO2 Adsorption Ability: Highly Efficient Photocatalysts for Artifical Photosynthesis. Catalysis Letters, 2015, 145, 640-646.	2.6	29
203	One-pot synthesis of bifunctionalized TiO2 mesoporous photocatalyst with visible light response. Journal of Porous Materials, 2015, 22, 313-319.	2.6	3
204	Hole-transport-material-free perovskite solar cells based on nanoporous gold back electrode. RSC Advances, 2015, 5, 58543-58548.	3.6	20
205	Constructing a High-Efficiency MoO ₃ /Polyimide Hybrid Photocatalyst Based on Strong Interfacial Interaction. ACS Applied Materials & Interfaces, 2015, 7, 14628-14637.	8.0	97
206	Hexahedron Prism-Anchored Octahedronal CeO ₂ : Crystal Facet-Based Homojunction Promoting Efficient Solar Fuel Synthesis. Journal of the American Chemical Society, 2015, 137, 9547-9550.	13.7	294
207	Catalytic reduction of NOx by CO over a Ni–Ga based oxide catalyst. Journal of Materials Chemistry A, 2015, 3, 15133-15140.	10.3	6
208	<i>In Situ</i> Fabrication of Highly Conductive Metal Nanowire Networks with High Transmittance from Deep-Ultraviolet to Near-Infrared. ACS Nano, 2015, 9, 2502-2509.	14.6	65
209	Double-shelled plasmonic Ag-TiO2 hollow spheres toward visible light-active photocatalytic conversion of CO2 into solar fuel. APL Materials, 2015, 3, .	5.1	59
210	Photocatalytic CO2 reduction of BaCeO3 with 4f configuration electrons. Applied Surface Science, 2015, 358, 463-467.	6.1	27
211	Rational construction of a CdS/reduced graphene oxide/TiO ₂ core–shell nanostructure as an all-solid-state Z-scheme system for CO ₂ photoreduction into solar fuels. RSC Advances, 2015, 5, 88409-88413.	3.6	71
212	Barium zirconate: a new photocatalyst for converting CO ₂ into hydrocarbons under UV irradiation. Catalysis Science and Technology, 2015, 5, 1758-1763.	4.1	44
213	Quantitative Analysis and Visualized Evidence for High Charge Separation Efficiency in a Solidâ€Liquid Bulk Heterojunction. Advanced Energy Materials, 2014, 4, 1301785.	19.5	88
214	Effects of Ba–O codoping on the photocatalytic activities of Ta ₃ N ₅ photocatalyst: a DFT study. RSC Advances, 2014, 4, 55615-55621.	3.6	9
215	Photocatalysis and Photoelectrochemistry for Solar Fuels. International Journal of Photoenergy, 2014, 2014, 1-2.	2.5	5
216	Formation mechanism of ZnS impurities and their effect on photoelectrochemical properties on a Cu2ZnSnS4 photocathode. CrystEngComm, 2014, 16, 2929.	2.6	41

#	Article	IF	CITATIONS
217	Highly Photoâ€Responsive LaTiO ₂ N Photoanodes by Improvement of Charge Carrier Transport among Film Particles. Advanced Functional Materials, 2014, 24, 3535-3542.	14.9	166
218	Photoconversion: Photocatalytic Conversion of CO ₂ into Renewable Hydrocarbon Fuels: Stateâ€ofâ€theâ€Art Accomplishment, Challenges, and Prospects (Adv. Mater. 27/2014). Advanced Materials, 2014, 26, 4598-4598.	21.0	7
219	Developing high-efficiency ï€ conjugated polymer semiconductor for photocatalytic degradation of dyes under visible light irradiation. RSC Advances, 2014, 4, 57153-57158.	3.6	28
220	Design and synthesis of cation-functionalized ionic liquid for application as electrolyte in proton exchange membrane fuel cells. Journal of Materials Chemistry A, 2014, 2, 19275-19281.	10.3	8
221	One-dimensional assembly of TiO ₂ nanoparticles toward enhancing light harvesting and electron transport for application in dye-sensitized solar cells. RSC Advances, 2014, 4, 10519-10524.	3.6	5
222	Polymeric g-C ₃ N ₄ Coupled with NaNbO ₃ Nanowires toward Enhanced Photocatalytic Reduction of CO ₂ into Renewable Fuel. ACS Catalysis, 2014, 4, 3637-3643.	11.2	580
223	Basic Molten Salt Route to Prepare Porous SrTiO ₃ Nanocrystals for Efficient Photocatalytic Hydrogen Production. European Journal of Inorganic Chemistry, 2014, 2014, 3731-3735.	2.0	19
224	Vitamin E assisted polymer electrolyte fuel cells. Energy and Environmental Science, 2014, 7, 3362-3370.	30.8	35
225	Cathodic shift of onset potential for water oxidation on a Ti ⁴⁺ doped Fe ₂ O ₃ photoanode by suppressing the back reaction. Energy and Environmental Science, 2014, 7, 752-759.	30.8	228
226	Nanostructured SnO2 photoanode-based dye-sensitized solar cells. Science Bulletin, 2014, 59, 2122-2134.	1.7	22
227	Photocurrent improvement in nanocrystalline Cu2ZnSnS4 photocathodes by introducing porous structures. Journal of Materials Chemistry A, 2013, 1, 15479.	10.3	50
228	Molecule-induced gradient electronic potential distribution on a polymeric photocatalyst surface and improved photocatalytic performance. Journal of Materials Chemistry A, 2013, 1, 5142.	10.3	35
229	A transparent Ti4+ doped hematite photoanode protectively grown by a facile hydrothermal method. CrystEngComm, 2013, 15, 2386.	2.6	42
230	Fiber dye-sensitized solar cells consisting of TiO2 nanowires arrays on Ti thread as photoanodes through a low-cost, scalable route. Journal of Materials Chemistry A, 2013, 1, 11790.	10.3	38
231	Photoelectrochemical cells for solar hydrogen production: current state of promising photoelectrodes, methods to improve their properties, and outlook. Energy and Environmental Science, 2013, 6, 347-370.	30.8	969
232	Tunable orange red phosphors: S ^{2â^'} -doped high temperature phase Ca ₃ SiO ₄ Cl ₂ :Eu ²⁺ for solid-state lighting. RSC Advances, 2013, 3, 1965-1969.	3.6	12
233	Zinc Gallogermanate Solid Solution: A Novel Photocatalyst for Efficiently Converting CO ₂ into Solar Fuels. Advanced Functional Materials, 2013, 23, 1839-1845.	14.9	89
234	An In Situ Simultaneous Reductionâ€Hydrolysis Technique for Fabrication of TiO ₂ â€Graphene 2D Sandwichâ€Like Hybrid Nanosheets: Grapheneâ€Promoted Selectivity of Photocatalyticâ€Driven Hydrogenation and Coupling of CO ₂ into Methane and Ethane. Advanced Functional Materials, 2013, 23, 1743-1749.	14.9	357

#	Article	IF	CITATIONS
235	Generalized synthesis of a family of multishelled metal oxide hollow microspheres. Journal of Materials Chemistry A, 2013, 1, 3575.	10.3	31
236	Water Adsorption and Decomposition on N/V-Doped Anatase TiO ₂ (101) Surfaces. Journal of Physical Chemistry C, 2013, 117, 6172-6184.	3.1	24
237	Versatile nanobead-scaffolded N-SnO2mesoporous microspheres: one-step synthesis and superb performance in dye-sensitized solar cell, gas sensor, and photocatalytic degradation of dye. Journal of Materials Chemistry A, 2013, 1, 524-531.	10.3	23
238	Versatile Grapheneâ€Promoting Photocatalytic Performance of Semiconductors: Basic Principles, Synthesis, Solar Energy Conversion, and Environmental Applications. Advanced Functional Materials, 2013, 23, 4996-5008.	14.9	335
239	Direct Growth of Fe ₂ V ₄ O ₁₃ Nanoribbons on a Stainlessâ€Steel Mesh for Visibleâ€Light Photoreduction of CO ₂ into Renewable Hydrocarbon Fuel and Degradation of Gaseous Isopropyl Alcohol. ChemPlusChem, 2013, 78, 274-278.	2.8	41
240	An Ionâ€Exchange Phase Transformation to ZnGa ₂ O ₄ Nanocube Towards Efficient Solar Fuel Synthesis. Advanced Functional Materials, 2013, 23, 758-763.	14.9	72
241	Innenrücktitelbild: A Co-catalyst-Loaded Ta3N5Photoanode with a High Solar Photocurrent for Water Splitting upon Facile Removal of the Surface Layer (Angew. Chem. 42/2013). Angewandte Chemie, 2013, 125, 11381-11381.	2.0	0
242	Simultaneous sensitization and hole activation in carbon nitride polymer sensitized TiO2. RSC Advances, 2012, 2, 5585.	3.6	18
243	A Theoretical Study of Water Adsorption and Decomposition on the Low-Index Stoichiometric Anatase TiO ₂ Surfaces. Journal of Physical Chemistry C, 2012, 116, 7430-7441.	3.1	70
244	Effects of Surface Electrochemical Pretreatment on the Photoelectrochemical Performance of Mo-Doped BiVO ₄ . Journal of Physical Chemistry C, 2012, 116, 5076-5081.	3.1	172
245	Interfacial modification of photoelectrode in ZnO-based dye-sensitized solar cells and its efficiency improvement mechanism. RSC Advances, 2012, 2, 7708.	3.6	26
246	ZnO plates synthesized from the ammonium zinc nitrate hydroxide precursor. CrystEngComm, 2012, 14, 154-159.	2.6	34
247	Zn ₂ GeO ₄ crystal splitting toward sheaf-like, hyperbranched nanostructures and photocatalytic reduction of CO ₂ into CH ₄ under visible light after nitridation. Journal of Materials Chemistry, 2012, 22, 2033-2038.	6.7	145
248	Unique Zn-doped SnO2 nano-echinus with excellent electron transport and light harvesting properties as photoanode materials for high performance dye-sensitized solar cell. CrystEngComm, 2012, 14, 6462.	2.6	64
249	Structure and Properties of Water on the Anatase TiO ₂ (101) Surface: From Single-Molecule Adsorption to Interface Formation. Journal of Physical Chemistry C, 2012, 116, 11054-11061.	3.1	64
250	Facile green synthesis of crystalline polyimide photocatalyst for hydrogen generation from water. Journal of Materials Chemistry, 2012, 22, 15519.	6.7	134
251	Robust Hollow Spheres Consisting of Alternating Titania Nanosheets and Graphene Nanosheets with High Photocatalytic Activity for CO ₂ Conversion into Renewable Fuels. Advanced Functional Materials, 2012, 22, 1215-1221.	14.9	373
252	Co ₃ O ₄ Nanoparticles as Robust Water Oxidation Catalysts Towards Remarkably Enhanced Photostability of a Ta ₃ N ₅ Photoanode. Advanced Functional Materials, 2012, 22, 3066-3074.	14.9	205

#	Article	IF	CITATIONS
253	Fabrication of hierarchically assembled microspheres consisting of nanoporous ZnO nanosheets for high-efficiency dye-sensitized solar cells. Journal of Materials Chemistry, 2012, 22, 14341.	6.7	57
254	Study on Platinum and Copper Nanosheets Alloys Supported on Mesoporous Titanium Dioxide Doped with Carbon Black as Electrocatalysts in PEM Fuel Cells. Electroanalysis, 2012, 24, 699-706.	2.9	8
255	Two-step reactive template route to a mesoporous ZnGaNO solid solution for improved photocatalytic performance. Journal of Materials Chemistry, 2011, 21, 5682.	6.7	29
256	Structure and energetics of low-index stoichiometric monoclinic clinobisvanite BiVO4 surfaces. RSC Advances, 2011, 1, 874.	3.6	58
257	Remarkable enhancement in photocurrent of In0.20Ga0.80N photoanode by using an electrochemical surface treatment. Applied Physics Letters, 2011, 99, .	3.3	27
258	BiVO4 nano–leaves: Mild synthesis and improved photocatalytic activity for O2 production under visible light irradiation. CrystEngComm, 2011, 13, 2500.	2.6	65
259	Solvothermal synthesis of monodisperse iron oxides with various morphologies and their applications in removal of Cr(vi). CrystEngComm, 2011, 13, 2727.	2.6	25
260	Solar hydrogen generation from seawater with a modified BiVO4 photoanode. Energy and Environmental Science, 2011, 4, 4046.	30.8	564
261	Sol–gel hydrothermal synthesis of visible-light-driven Cr-doped SrTiO3 for efficient hydrogen production. Journal of Materials Chemistry, 2011, 21, 11347.	6.7	157
262	A quick and green approach to prepare [Rmim]OH and its application in hydrophilic ionic liquid synthesis. New Journal of Chemistry, 2011, 35, 1661.	2.8	11
263	Microwave Hydrothermal Synthesis, Structural Characterization, and Visible-Light Photocatalytic Activities of Single-Crystalline Bismuth Ferric Nanocrystals. Journal of the American Ceramic Society, 2011, 94, 2688-2693.	3.8	75
264	Photophysical and photocatalytic properties of novel Y2GaSbO7 and Y2YbSbO7 photocatalysts under visible light irradiation. Journal of Materials Science, 2011, 46, 813-823.	3.7	11
265	Photoreduction of Carbon Dioxide Over NaNbO3 Nanostructured Photocatalysts. Catalysis Letters, 2011, 141, 525-530.	2.6	118
266	Surface modification of hematite photoanode films with rhodium. Rare Metals, 2011, 30, 38-41.	7.1	6
267	Immobilization of hemoglobin within channel of mesoporous TiO2-SiO2 composite. Rare Metals, 2011, 30, 144-146.	7.1	0
268	Design and theoretical analysis of resonant cavity for second-harmonic generation with high efficiency. Applied Physics Letters, 2011, 98, 031102.	3.3	9
269	Growth of Inâ€rich and Gaâ€rich InGaN alloys by MOCVD and fabrication of InGaNâ€based photoelectrodes. Physica Status Solidi C: Current Topics in Solid State Physics, 2010, 7, 1817-1820.	0.8	16
270	Influence of measurement parameter on dye-sensitized solar cell efficiency. , 2010, , .		0

#	Article	IF	CITATIONS
271	Facile synthesis of anatase TiO2 mesocrystal sheets with dominant {001} facets based on topochemical conversion. CrystEngComm, 2010, 12, 3425.	2.6	54
272	Improved photoelectrochemical responses of Si and Ti codoped α-Fe2O3 photoanode films. Applied Physics Letters, 2010, 97, .	3.3	105
273	Effect of crystal growth on mesoporous Pb3Nb4O13 formation, and their photocatalytic activity under visible-light irradiation. Journal of Materials Chemistry, 2010, 20, 2865.	6.7	19
274	Increasing the Oxygen Vacancy Density on the TiO ₂ Surface by La-Doping for Dye-Sensitized Solar Cells. Journal of Physical Chemistry C, 2010, 114, 18396-18400.	3.1	166
275	Polymerizable complex synthesis of BaZr1â [~] xSnxO3 photocatalysts: Role of Sn4+ in the band structure and their photocatalytic water splitting activities. Journal of Materials Chemistry, 2010, 20, 6772.	6.7	52
276	NaNbO3 Nanostructures: Facile Synthesis, Characterization, and Their Photocatalytic Properties. Catalysis Letters, 2009, 132, 205-212.	2.6	96
277	Multilayer structure with gradual increasing porosity for dye-sensitized solar cells. Applied Physics Letters, 2009, 94, 031905.	3.3	41
278	Photooxidation of Polycyclic Aromatic Hydrocarbons over NaBiO3 under Visible Light Irradiation. Catalysis Letters, 2008, 122, 131-137.	2.6	31
279	Correlation of Crystal Structures, Electronic Structures, and Photocatalytic Properties in a Series of Ag-based Oxides:  AgAlO ₂ , AgCrO ₂ , and Ag ₂ CrO ₄ . Journal of Physical Chemistry C, 2008, 112, 3134-3141.	3.1	152
280	Stable response to visible light of InGaN photoelectrodes. Applied Physics Letters, 2008, 92, 262110.	3.3	50
281	Photocatalytic properties of MIn(WO4)2 (M = Li, Na, and K). Journal of Materials Research, 2007, 22, 958-964.	2.6	5
282	Structural characterization and photocatalytic properties of novel Bi2FeVO7. Research on Chemical Intermediates, 2007, 33, 487-500.	2.7	12
283	Sol-gel synthesis and characterization of the photocatalyst BaCo1/3Nb2/3O3. Journal of Materials Science, 2006, 41, 1131-1135.	3.7	7
284	Enhanced photoelectrolysis of water with photoanode Nb:SrTiO3. Applied Physics Letters, 2004, 85, 689-691.	3.3	34